Structural Diversity and Superconductivity in S-P-H Ternary Hydrides Under Pressure

Nisha Geng, Tiange Bi, and Eva Zurek*

Department of Chemistry, State University of New York at Buffalo, Buffalo, NY 14260-3000, USA

E-mail: ezurek@buffalo.edu

*To whom correspondence should be addressed

Abstract

Evolutionary structure searches revealed a plethora of stable and low-enthalpy metastable phases in the S-P-H ternary phase diagram under pressure. A wide variety of crystalline structure types were uncovered ranging from those possessing one-dimensional chains, two-dimensional sheets based on S-H or S-P-H square lattices as well as S-H or P-H honeycombs, and cage-like structures. Some of the cage-like structures could be derived from doping the high-pressure high-temperature superconducting $Im\bar{3}m$ H_3S phase with phosphorous. Most of the discovered compounds were metallic, however those derived from $Im\bar{3}m$ H_3S lattices with low levels of P-doping were predicted to possess the highest superconducting critical temperatures (T_cs). The propensity for phosphorous to assume octahedral coordination, as well as the similar radii of sulfur and phosphorous are key to maintaining a high density of states at the Fermi level in $Im\bar{3}m$ $S_{0.875}P_{0.125}H_3$, whose T_c was estimated to be similar to that of H_3S at 200 GPa.

Introduction

The recent successes in the search for materials with ever-higher superconducting critical temperatures (T_cs) can be traced back to ideas planted by the late Neil Ashcroft. Building on his earlier prediction of phonon-mediated high-temperature superconductivity in metallic hydrogen,[1] in 2004 Ashcroft elegantly showed how chemical doping may be employed to decrease the pressure required to reach a metallic and superconducting state.[2] This proposal ultimately led to the experimental discovery of superconductivity in H_3S,[3] LaH_{10},[4,5] YH_6,[6,7] YH_9[7,8] and room temperature superconductivity in an unknown C-S-H phase.[9]

Because of the experimental difficulties inherent in high pressure research, theoretical calculations have been integral in suggesting targets for synthesis and for interpreting experimental measurements.[10,11] Advances in *ab initio* crystal structure prediction techniques and computational methods to approximate T_c have enabled the *in silico* search for superconductivity in high pressure hydrides.[12] By now, the phase diagrams of most binary hydrides have been explored computationally.[13–15] Ternary hydrides are the next frontier, however the combinatorial possibilities, potential for large unit cells, and role of metastability results in many challenges.[16,17]

One way that new ternary superconductors could potentially be made is by combining two binary hydrides that are thought to be good superconductors. For example, the extraordinary T_c values predicted for CaH_6[18] and measured for SH_3[3,19] inspired the computational search for superconductivity in $Ca_xS_yH_z$ phases.[20] A $P\bar{6}m2$ $CaSH_3$ compound built from CaH_2 layers separated by honeycomb H-S layers was predicted to have a T_c reaching 100 K at 128 GPa. Inspired by the prediction of high T_c in metal superhydrides with clathrate cages,[21,22] the (La/Y)H_{10} and (La/Y)H_6 ternaries were synthesized, and their maximum measured T_cs were 253 and 237 K, respectively.[23] Another strategy that could be used to find promising ternary superconductors is to begin with a binary phase known to have a large T_c and dope it with a third (or fourth) element. The doping could potentially increase T_c (c.f. Li_2MgH_{16}[24] versus MgH_{16}[25]) or extend the region of phase stability to lower pressures (c.f. $LaBH_8$[26,27] or $LaBeH_8$[28] versus LaH_{10}[21,22]).

It has been proposed that doping can be employed to tune the position of the Fermi level

(E_F) so that it lies on a maximum in the density of states (DOS) thereby increasing the electron phonon coupling parameter, λ, and concomitantly the T_c. This mechanism ought to be particularly useful for enhancing the T_c in H_3S, whose E_F is just shy of the top of a peak caused by the presence of two van Hove singularities (vHs) that straddle E_F. Computations using the virtual crystal approximation (VCA), which creates alchemical atoms whose properties vary smoothly upon doping, have explored the effect of doping on the T_c of H_3S. Heil and Boeri found that T_c could be enhanced by replacing sulfur by more electronegative elements such as oxygen or halogen atoms,[29] whereas Ge *et al.* and Hu *et al.* concluded that T_cs above the freezing point of water could be obtained by low dopings of phosphorous,[30] silicon,[30,31] and most recently carbon.[31,32] However, other VCA-based studies found that partial substitution of sulfur with another p-block element did not enhance T_c significantly, or not at all.[33,34]

The VCA model is advantageous since it enables the study of low doping levels that can only be modelled by large unit cells whose T_cs cannot be computed from first principles because of the immense expense. At the same time, the VCA assumes the band structure will not be perturbed by doping, and only the position of E_F will change (rigid band model). Recent theoretical studies have called this assumption into question. For example, calculations on $C_xS_{1-x}H_3$ and $C_xS_{1-x}H_{3+x}$ supercells with doping levels ranging from 1.85-25% illustrated that incorporation of carbon into the H-S lattice decreases the number of bands at E_F by breaking degeneracies and localizing electrons in covalent C-H bonds.[35] Calculations on phases where half of the SH_3 units were substituted by methane resulting in a CSH_7 stoichiometry, yielded maximal T_cs of 181 K at 100 GPa[36]and 194 K at 150 GPa.[37] Theory has shown that Se[38,39] and Cl[40,41] dopings do not raise the superconducting critical temperature of H_3S. And, phosphorous dopings have been shown to both increase and decrease its T_c. For example, a 6.25% phosphorus doping resulted in a T_c of 212 K[40] or 262 K at 200 GPa,[41] a 12.5% phosphorus doped structure was predicted to possess a T_c of 194 K at 200 GPa[40] or 190 K at 155 GPa,[42] and a 50.0% phosphorus doped structure yielded a T_c of 89 K at 200 GPa[43] or 157 K at 155 GPa.[42] Another drawback of both the VCA[30,33] and the supercell models with S$\rightarrow$P substitutions[40–42] is that they did not explore the potential energy

landscape for the compositions considered, and the S-P-H ratios were fixed. Moreover, the studies carried out with both methods employed structures derived from $Im\bar{3}m$ or $R3m$ H_3S cells, which may not form in experiment, especially if other novel S-P-H ternary phases are thermodynamically preferred.[12]

To overcome these limitations, herein we perform a thorough theoretical study that employs crystal structure prediction techniques to identify the most stable ternary phases for a wide $S_xP_yH_z$ composition range. The electronic structure including the density of states, electron localization functions, electronic and phonon band structures are analyzed. Four different families of structures including those comprised of cages, two dimensional sheets with hexagonal or other motifs, and one-dimensional molecular chains are found. Unlike our previous results on carbon doping of H_3S, here we find at least one system where phosphorous doping does not decrease the DOS at E_F. This $Im\bar{3}m$ S_7PH_{24} compound is estimated to have a T_c comparable to its parent $Im\bar{3}m$ H_3S structure at 200 GPa. We hope our study can guide the experimental discovery and characterization of new ternary superconducting S-P-H compounds under pressure.

Methods

Crystal structure prediction (CSP) searches were performed to find stable and low enthalpy metastable phases with SPH_n ($n = 1 - 8$), S_xPH and SP_yH ($x, y = 2, 3$) stochiometries, as well as those corresponding to phosphorus doped H_3S phases at 100, 150 and 200 GPa using 1-4 formula units in the simulation cell. The stoichiometries of the doped phases we considered were $S_xP_{1-x}H_3$ ($x = 0.125, 0.2, 0.25, 0.33, 0.4, 0.6, 0.67, 0.75, 0.8$), which were modelled by S_7PH_{24}, S_4PH_{15}, S_3PH_{12}, S_2PH_9, $S_3P_2H_{15}$, $S_2P_3H_{15}$, SP_2H_9, SP_3H_{12}, and SP_4H_{15} cells, respectively. In this case the EA searches were seeded with doped supercells from the previously reported $Im\bar{3}m$ H_3S and $R3m$ H_3S structures.[19] We focused on H_3S where some of the sulfur atoms were replaced by phosphorous atoms because this type of doping may move E_F so that it sits on top of a peak in the DOS thereby resulting in a phase with a T_c that surpasses that of H_3S. Similar stoichiometries

were considered in a study undertaken to determine the effect of replacing S by Se on the T_c of the resulting $S_xSe_{1-x}H_3$ phases.[38] In addition, we considered ternary compounds with the general formula $S_xP_yH_z$ where two of x, y or z were fixed and the third was varied. We did not expect these compounds to have particularly high T_cs, since their electronic structure would differ significantly from that of $S_xP_{1-x}H_3$, but considered them in case they may lie on the convex hull. While a more thorough search of composition space would better map out the convex hull, the main purpose of our study was to uncover compounds with particularly high T_c values.

The CSP searches were performed using the open-source evolutionary algorithm (EA) XTALOPT[44–46] version 12.[47] The initial generation consisted of random symmetric structures that were created by the RANDSPG algorithm,[48] and the minimum interatomic distance between S-S, S-H, S-P, H-H, H-P, and P-P atoms were constrained to 0.88, 0.71, 0.93, 0.53, 0.76 and 0.98 Å using a uniform scaling factor of 0.5 multiplied by tabulated covalent radii. Duplicate structures were identified via the XTALCOMP algorithm[49] and discarded from the breeding pool. The lowest enthalpy structures in each EA run were relaxed from 100 to 200 GPa and their relative enthalpies and equations of states are given in the Supplementary Information Figs. S1-6.

Geometry optimizations and electronic structure calculations including band structures, the densities of states (DOS), electron localization functions (ELFs), and Bader charges were carried out using density functional theory (DFT) as implemented in the Vienna *ab-initio* Simulation Package (VASP) version 5.4.1,[50,51] with the gradient-corrected exchange and correlation functional of Perdew-Burke-Ernzerhof (PBE).[52] The crystal orbital Hamilton population (COHP) and the negative of the COHP integrated to the Fermi level (-iCOHP) was calculated using the LOBSTER package to analyze the bonding of selected phases.[53]

The projector augmented wave (PAW) method[54] was employed, and the S $3s^2 3p^4$, P $3s^2 3p^3$ and H $1s^1$ electrons were treated explicitly in all of the calculations. The plane-wave basis set energy cutoffs were 350-400 eV in the EA searches and 700 eV in precise geometry optimizations. The k-point meshes were generated using the Γ-centered Monkhorst-Pack scheme, while the number of divisions along each reciprocal lattice vector was selected so that the product of this number with

the real lattice constant was 30 Å in the EA searches and 50 Å for precise geometry optimizations.

Phonon calculations were carried out via the supercell approach[55,56] using the VASP package coupled to the PHONOPY code.[57] The electron-phonon coupling (EPC) calculations were carried out using the Quantum Espresso (QE) program.[58] The S $3s^2 3p^4$, P $3s^2 3p^3$ and H $1s^1$ pseudopotentials were obtained from the PSlibrary,[59] and generated by the method of Trouiller-Martins.[60] The plane-wave basis set energy cutoffs were chosen to be 60 Ry. The Brillouin zone sampling scheme of Methfessel-Paxton[61] was applied. The EPC parameter, λ, was calculated using a set of Gaussian broadenings with an increment of 0.005 Ry from 0.0 to 0.500 Ry. The broadening for which λ was converged to within 0.05 Ry is provided in Table S5, along with the k and q grids that were deemed to be converged. The T_c was estimated using the Allen-Dynes modified McMillan equation[62] with a renormalized Coulomb potential, μ^*, of 0.1. For phases with λ greater than 1.3 more accurate estimates of the T_c were also calculated by numerically solving the Eliashberg equations.[63]

Results and Discussion

The enthalpies of formation, ΔH_F, of the most stable S-P-H ternary phases found in our EA searches for a given stoichiometry at 100, 150 and 200 GPa were calculated and employed to construct the convex hull. If the ΔH_F of a structure falls on the convex hull, it is a thermodynamically stable phase. However, previous theoretical and experimental work on binary hydrides has illustrated that synthesizability is not only determined by the ΔH_F estimated within the static lattice approximation. It turns out that the synthesis pathway, which includes the choice of the precursors and annealing schemes, is also key in determining the products that are formed. For example, despite the fact that Ca_2H_5 lies 20 meV/atom above the convex hull, this binary hydride has been synthesized.[77] Moreover, even though DFT calculations predict that hydrides of phosphorous are not thermodynamically stable under pressure,[78–80] a superconducting PH_n phase[81] and a van der Waals $(PH_3)_2H_2$ crystalline compound[82] have been synthesized. Moreover, a number of H_xS_y superconductors have been made,[83] and various stoichiometries including H_3S,[19,84] H_2S,[85,86] HS_2,[75]

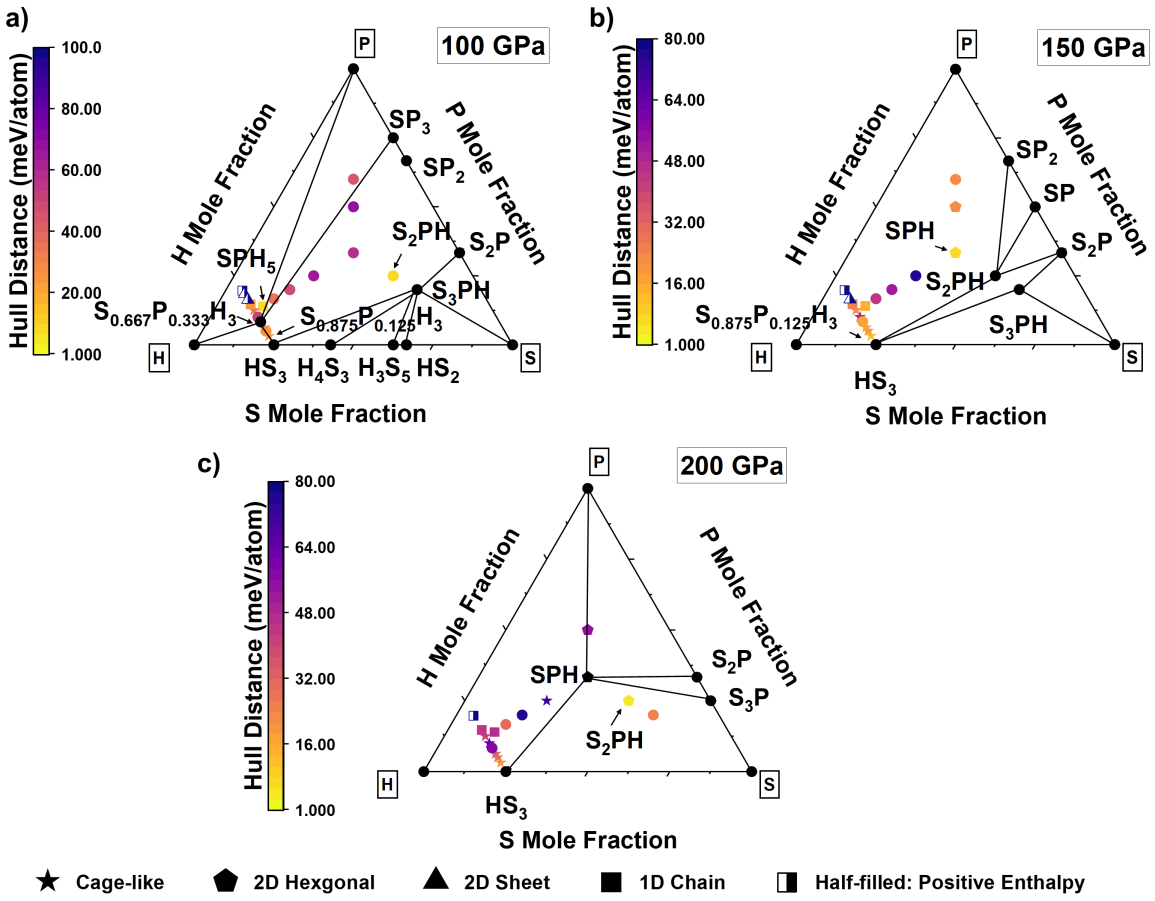

Figure 1: Distance from the convex hull of the S-P-H phases considered with respect to elemental S, P, and ½ H_2 as computed with the PBE functional at 100, 150, and 200 GPa. The thermodynamically stable phases are shown in black while the metastable phases are represented by different colors based on their distance from the hull. The phases with positive enthalpies are shown with a hall-filled shape. The phases containing special geometrical motifs such as cage-like structures, 2D hexagonal or other sheets, and 1D chains are labelled as stars, pentagons, triangles, and squares, respectively. ΔH_F was calculated using the enthalpies of the experimentally or theoretically known structures: simple cubic (sc, 100 GPa)[64–66] and simple hexagonal (sh, 150–200 GPa)[66] for P; $P6_3/m$ (100 GPa)[67] and $C2/c$ (150–200 GPa)[67] for H; β-Po[68] for S (100–200 GPa) since the crystal structure of S above 83 GPa is still disputed;[69–71] $C2/c$ (200 GPa) for S_3P;[72] $C2/m$ (100–150 GPa) and $P\bar{3}m1$ (200 GPa) for S_2P;[72] $P2_1/m$ (150 GPa) for SP;[72] $C2/m$-I (100 GPa) and $C2/m$-II (150 GPa) for SP_2;[72] $C2/m$ (100 GPa) for SP_3;[72] $C2/c$ (100 GPa), $R3m$ (150 GPa), and $Im\bar{3}m$ (200 GPa) for H_3S;[3,19,73] $Pbcm$ (100 GPa) and $C2c$ (150–200 GPa) for HS_2;[74,75] $Pnma$ (100 GPa) for H_4S_3;[73] $C2/m$ (100 GPa) for H_3S_5.[76]

H_4S_3,[73] H_5S_2,[87] exotic Magnéli phases,[88] and self-ionized $(SH^-)(H_3S)^+$ perovskites[89] that may have long modulations[90,91] have been proposed. Because metastable binary S-H and P-H phases have been synthesized, herein we have chosen to analyze structures that fall on the convex hull (Fig. 1), as well as several metastable phases with unique structural characteristics that are within the realm of synthesizability.

At 100 GPa both S_2PH_9, which can be considered a P-doped H_3S phase with a $S_{0.67}P_{0.33}H_3$ composition, and S_3PH lie on the hull. In addition to S_3PH, S_2PH also comprises the 150 GPa hull, whereas only SPH falls on the hull at 200 GPa. Noteably, most of the compositions studied were within the 70 meV/atom threshold corresponding to the 90$^{\text{th}}$ percentile of DFT-calculated metastability for inorganic crystalline materials at 1 atm,[92] but the ΔH_F for three phosphorus-rich compounds, SP_2H_9 ($S_{0.33}P_{0.67}H_3$), SP_3H_{12} ($S_{0.25}P_{0.75}H_3$) and SP_4H_{15} ($S_{0.2}P_{0.8}H_3$), were positive with respect to the elemental phases at all pressures. SP_3H was also unstable with respect to H_2, P and S at 200 GPa. The structural parameters and the distance from the convex hull for all S-P-H ternary phases considered are provided in Table S6-8 and S2, respectively. Moreover, the files have been uploaded to the NOvel MAterials Discovery (NOMAD) repository and archive.[93]

Because the enthalpy of formation of the binary hydrides of phosphorous is positive above 40 GPa,[78–80] none of the previously predicted phases are plotted on Fig. 1. For the hydrides of sulfur the $C2/c$ H_3S,[73] $Pnma$ H_4S_3,[73] $Pbcm$ HS_2[74] and $C2/m$ H_3S_5[76] phases were employed to construct the 100 GPa hull, while $R3m$ and $Im\bar{3}m$ H_3S[19] were used to build the 150 and 200 GPa hulls, respectively. For the P-S phases we employed structures previously identified via crystal structure prediction:[72] $C2/m$ SP_3, $C2/m$-I SP_2 and $C2/m$ S_2P lay on the 100 GPa hull; $C2/m$-II SP_2, $P2_1/m$ SP and $C2/m$ S_2P lay on the hull at 150 GPa; $P\bar{3}m1$ S_2P and $C2/c$ S_3P lay on the hull at 200 GPa.

In our work we found stable and metastable ternary S-P-H species with a variety of distinct structural motifs including: (i) cage-like geometries, e.g. S_7PH_{24} ($S_{0.875}P_{0.125}H_3$), S_4PH_{15} ($S_{0.8}P_{0.2}H_3$), S_3PH_{12} ($S_{0.75}P_{0.25}H_3$), $S_3P_2H_{15}$ ($S_{0.6}P_{0.4}H_3$), SPH_6 ($S_{0.5}P_{0.5}H_3$) and SPH_2; (ii) two-dimensional hexagonal sheets, e.g. S_2PH and SP_2H; (iii) other types of two-dimensional sheets,

e.g. $P\bar{1}$ SP_2H_9 ($S_{0.33}P_{0.67}H_3$) and SP_3H_{12} ($S_{0.25}P_{0.75}H_3$); and (iv) one-dimensional chains, e.g. SPH_5, $S_2P_3H_{15}$ ($S_{0.4}P_{0.6}H_3$) and SP_4H_{15} ($S_{0.2}P_{0.8}H_3$). We also studied other thermodynamically stable phases (e.g. S_3PH and S_2PH_9 ($S_{0.67}P_{0.33}H_3$)), and other superconducting phases (e.g. SPH_3 and SPH_4). The structural peculiarities of many of these are described in the following sections to showcase the rich potential energy landscape and geometrical complexity that is possible. However, for brevity we do not discuss dynamically stable phases that either did not possess any distinct structural motifs, or those that are only slight variations of presented phases. Information on some of these, e.g. SPH_n $(n = 3 - 5)$ and SP_4H_{15} ($S_{0.2}P_{0.8}H_3$), can be found in Fig. S42.

Table 1: ΔH (meV/atom) for the reaction $H_3S + xP \rightarrow H_3S_{1-x}P_x + xS$ for different doping levels, x, at various pressures. The enthalpy of the $C2/c$, $R3m$, and $Im\bar{3}m$ H_3S phases was chosen to calculate the ΔH at 100, 150, and 200 GPa, respectively. The phases employed for P and S are the same as those listed in the caption to Figure 1.

P/x	12.5%[a]	20%[a]	25%[a]	33%[b]	40%[a]	50%[a]	60%[c]	67%[c]	75%[c]	80%[d]
100	34.3 (23.9[e])	41.5	87.4	48.1	N/A	82.1	133.0	119.4	139.1	79.8
150	26.6 (31.2[e])	43.4	96.4	47.4	57.2	93.7	136.3	120.2	147.0	79.5
200	40.0 (36.5[e]/37.0[f])	55.3	116.2	66.1	100.7	123.1	149.7	142.7	175.6	107.1

[a] Illustrated in Fig. 2
[b] Illustrated in Fig. 6
[c] Illustrated in Fig. 5
[d] Illustrated in Fig. S42
[e] Ref.[40]
[f] Ref.[41]

To guage the stability of the P doped phases, we considered the enthalpy of the reaction $H_3S + xP \rightarrow H_3S_{1-x}P_x + xS$ (Table 1). Our results for $S_{0.875}P_{0.125}H_3$ (S_7PH_{24}) were similar to those calculated for the same stoichiometry by Nakanishi and co-workers.[40] The relatively small positive ΔH values suggest that this phase could potentially be synthesized, especially if configurational entropy is able to overcome the enthalpic penalty, as is the case for numerous multicomponent systems.[94] Generally speaking, as the doping level increases, the ternaries become progressively destabilized with the sulfur-rich and phosphorours-rich phases possessing ΔH values ranging from 26.6-116.2 meV/atom and 79.8-175.6 meV/atom, respectively. S_2PH_9 ($S_{0.67}P_{0.33}H_3$), and $S_3P_2H_{15}$ ($S_{0.6}P_{0.4}H_3$), whose structural peculiarities will be discussed below, did not follow this trend.

Cage Like Structures

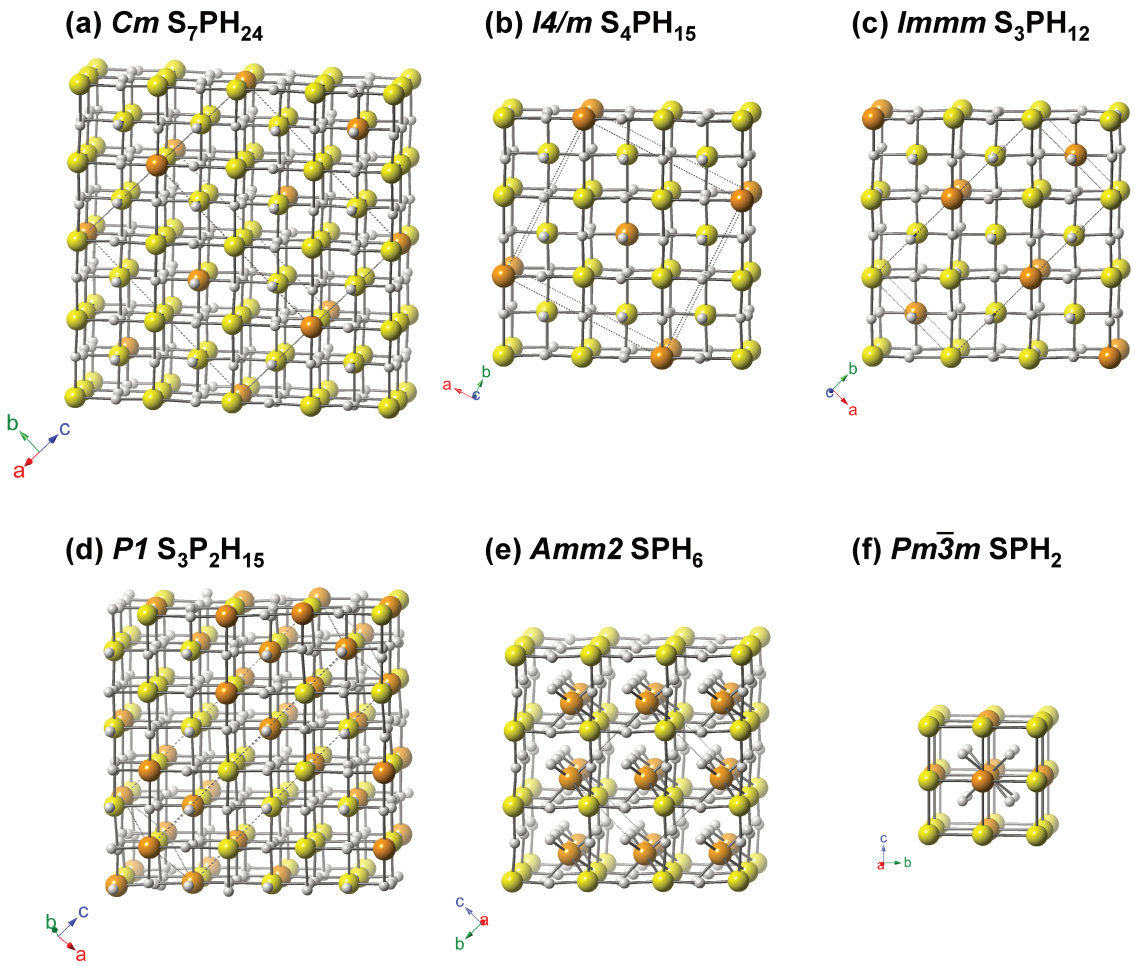

Figure 2: Illustrations of predicted S-P-H phases with cage-like structures: (a) Cm S_7PH_{24} ($S_{0.875}P_{0.125}H_3$) at 150 GPa, (b) $I4/m$ S_4PH_{15} at 200 GPa, (c) $Immm$ S_3PH_{12} at 200 GPa , (d) $P1$ $S_3P_2H_{15}$ at 150 GPa, (e) $Amm2$ SPH_6 at 150 GPa, and (f) $Pm\bar{3}m$ SPH_2 at 200 GPa. S/P/H atoms are colored yellow/orange/white.

The discovery of record breaking T_c in H_3S is a milestone in the search for room-temperature superconducting materials. Theoretical calculations predicted that $Im\bar{3}m$ H_3S is the most stable phase at 200 GPa with a T_c of 191-204 K,[19] in-line with independent experiments that measured a T_c of 203 K when hydrogen sulfide was compressed to 155 GPa.[3] The S atoms in $Im\bar{3}m$ H_3S,

which are separated symmetrically by hydrogen atoms, form a bcc lattice. Another structurally related H_3S phase with $R3m$ symmetry, which contains a pyramidal H_3S unit with a calculated T_c of 155-166 K at 130 GPa, was also proposed.[19] Therefore, we seeded all of our $S_xP_{1-x}H_3$ EA searches with supercells of both $Im\bar{3}m$ and $R3m$ H_3S where some of the sulfur atoms were replaced by phosphorous atoms. Several cage-like structures including S_7PH_{24} ($S_{0.875}P_{0.125}H_3$), S_4PH_{15} ($S_{0.8}P_{0.2}H_3$), S_3PH_{12} ($S_{0.75}P_{0.25}H_3$), $S_3P_2H_{15}$ ($S_{0.6}P_{0.4}H_3$), SPH_6 ($S_{0.5}P_{0.5}H_3$) and SPH_2, which resembled $Im\bar{3}m$ and $R3m$ H_3S, were found and are discussed below (see Fig. 2).

A Cm S_7PH_{24} ($S_{0.875}P_{0.125}H_3$) structure with 1 forumula unit in the primitive cell was found via CSP, and it also possessed the lowest enthalpy at 100 GPa. This phase lay only 24.5 and 12.2 meV/atom above the convex hull at 100 and 150 GPa, respectively. It could be viewed as a distorted version of the $R3m$ cell considered by Nakanishi,[40] and the distortion stabilized the structure by 14.9 and 7.0 meV/atom at 100 and 150 GPa, respectively. By 200 GPa the high-symmetry $Im\bar{3}m$ phase became preferred, and it lay 23.6 meV/atom above the convex hull. The Cm phase contained SH_3 and SH_4 structural motifs, along with PH_6 units whose geometry deviated ever-so-slightly from ideal octahedral coordination. In the higher pressure $Im\bar{3}m$ phase these motifs were forced close enough to each other so they formed multi-centered bonds where every S and P atom was octahedrally coordinated with SH-P and PH-S distances of 1.462 and 1.522 Å, respectively, at 200 GPa. The HS-H distances in this phase were the same as within $Im\bar{3}m$ H_3S at the same pressure, 1.492 Å. The Bader charge on the PH_6 unit within S_7PH_{24} was calculated to be -0.09e at 150 GPa and 0.03e at 200 GPa.

Our calculations show that the peak in the DOS of H_3S lies 0.28 eV below E_F at 200 GPa. Assuming a rigid band model, this peak could be accessed by $\sim$12% P doping, which corresponds well to the $S_{0.875}P_{0.125}H_3$ stoichiometry (Fig. 3). In contrast to our results on H_3S with low levels of S$\rightarrow$C and $SH_3\rightarrow CH_4$ replacements,[35] the DOS at E_F ($g(E)$/Å^3) within $Im\bar{3}m$ S_7PH_{24} is about the same as that of the undoped binary. A Bader analysis, which typically underestimates the formal charge, suggested a charge of +0.25 on CH_6, whereas PH_6 is nearly neutral. Moreover, a plot of the electron localization function (ELF) is indicative of the formation of multicentered P-H-S

bonds, whereas the ELF plot for O_h-$CS_{15}H_{48}$ suggested the presence of strong C-H bonds, with the positively charged CH_6 motif weakly interacting with the nearby sulfur atoms. The different behavior of P versus C doping can be traced back to their elemental properties. The atomic radius of phosphorus (98 pm) is slightly larger than that of sulfur (87 pm), but the radius of carbon is markedly smaller (67 pm). Moreover, whereas the electronegativity of sulfur and carbon is about the same, phosphorous is somewhat less adept at attracting electrons. As a result, low levels of P-doping have a markedly different effect on the electronic structure of H_3S as compared to small amounts of C-doping. This finding suggests that choosing the right element for chemical substitution is key towards designing a material with an electronic structure that is particularly conducive towards superconductivity.

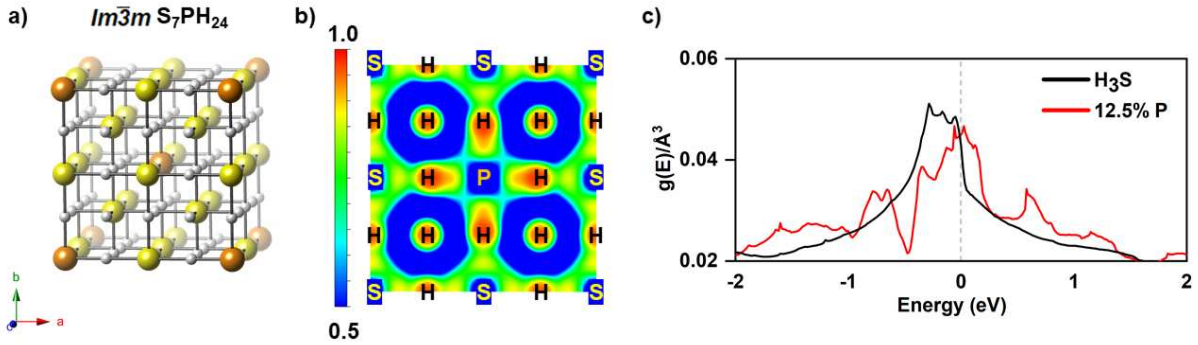

Figure 3: (a) $Im\bar{3}m$ S_7PH_{24} ($S_{0.875}P_{0.125}H_3$) at 150 GPa. (b) The Electron Localization Function (ELF) contour plotted in a plane that bisects the S-H-P contacts. (c) The density of states (DOS) plot near the Fermi (E_F) level of $Im\bar{3}m$ H_3S (black) and $Im\bar{3}m$ S_7PH_{24} (red) at 200 GPa. The value of the DOS at E_F is 0.043 and 0.045 states $eV^{-1}/Å^3$ (0.063 and 0.067 states eV^{-1}/valence electron), respectively.

To further interrogate the bonding in the P-doped structure the negative of the crystal orbital Hamilton population integrated to the Fermi level (-iCOHP) was calculated. In Cm S_7PH_{24} at 150 GPa five of the P-H bonds were stronger than the S-H bonds (4.18-4.23 eV/bond versus 1.97-2.12 eV/bond) and one bond was about the same strength (3.44 versus 3.13 eV/bond). Higher pressures promote multi-centered bonding so that in $Im\bar{3}m$ S_7PH_{24} at 200 GPa the PH-S and SH-P -iCOHPs were almost equivalent (3.22 versus 3.74 eV/bond), and quite comparable to the bond

strength within undoped $Im\bar{3}m$ H_3S at this pressure (3.67 eV/atom). Again, this differs markedly from our previous results, which showed that carbon doping decreased the CH-S bond strength to 2.00 eV/bond. Because P-doping does not perturb the structure nor the electronic structure of the H_3S lattice to the same degree as C-doping, it does not decrease the metallicity of H_3S significantly, or at all, and the electrons remain delocalized throughout the S-P-H lattice at 200 GPa. In contrast to our previous findings on S→C substitutions in an octahedral coordination environment,[35] which decreased the T_c from 174 to 130 K at 270 GPa, we would therefore expect the T_c of $Im\bar{3}m$ S_7PH_{24} to be closer to that of $Im\bar{3}m$ H_3S at 200 GPa, and perhaps even to surpass it. This hypothesis will be tested below.

S_4PH_{15} ($S_{0.8}P_{0.2}H_3$) possesed the second highest S-concentration of the doped $S_{1-x}P_xH_3$ phases that were considered. $P1$, $I4$, and $I4/m$ symmetry structures were the most stable at 100, 150, and 200 GPa, respectively, and they lay only 25.7, 20.2, and 29.0 meV/atom above the convex hull at these pressures. $P1$ S_4PH_{15} contains four H_2, one PS_2H_2 and one $(SH_2)_2H$ unit in the primitive cell. We do not show it in Fig. 2 since it is not a cage-like structure, and it is semiconducting at 100 GPa. The $I4$ and $I4/m$ symmetry phases are related to each other, and both can be considered as cage-like structures similar to Cm S_7PH_{24}. At 150 GPa the H-S distances measured 1.415-1.667 Å, shortening slightly to 1.412-1.590 Å at 200 GPa (c.f. 1.492 Å in $Im\bar{3}m$ H_3S at 200 GPa). The ideal octahedral geometry about the P atom was somewhat distorted in the $I4/m$ phase with four P-H bonds measuring 1.427 Å, and the remaining two measuring 1.483 Å. Lowering the pressure induces further distortions from the ideal octahedral coordination environment in both the H-P-H angles (89.9-90.1°) and P-H distances (1.437/1.485/1.580 Å).

For the S_3PH_{12} ($S_{0.75}P_{0.25}H_3$) stoichiometry, two metastable cage-like structures with $Imm2$ (100-190 GPa) and $Immm$ (200 GPa) symmetries were found with a distance of 28.4, 18.5, 33.2 meV/atom above the convex hull at 100, 150, and 200 GPa, respectively. The $Immm$ phase was also identified at 200 GPa by Tsuppayakorn-aek et al.,[43] but the $Imm2$ was not reported before. At 150 GPa the S-H distances ranged from 1.386-1.711 Å, and increasing pressure decreased this range (1.422-1.613 Å at 200 GPa). The geometry about the P atom deviated somewhat from that

of a perfect octahedron with four short and two long P-H distances (1.417 and 1.483 Å at 200 GPa, and 1.422 Å, 1.476 and 1.588 Å at 150 GPa). The DOS at E_F of these two metallic phases was somewhat lower than for 12.5% doping.

Several other dynamically stable cage-like structures with larger P-dopings were also found: $P1$ $S_3P_2H_{15}$ (stable between 150-200 GPa), $Amm2$ SPH_6 (stable between 100-200 GPa), and $Pm\bar{3}m$ SPH_2 (stable at 200 GPa). Their distance from the convex hull was typically somewhat larger than that of the aforementioned phases (Table S2), but still within the realm of synthesizability. Therefore, their structural peculiarities and electronic structures are also briefly described. Whereas, $P1$ $S_3P_2H_{15}$ can still be viewed as a perturbation of a doped H_3S parent, larger phosphorous content has a profound impact on the geometries of the most stable structural alternatives. For a 1:1 chalcogen to pnictogen ratio CSP identified an $Amm2$ SPH_6 phase that was built from a 2D square S-H net where the sulfur atoms lay on the corners, and the hydrogen atoms bisected the edges. A layer of PH_4 units separated the layers, with the phosphorous atoms forming additional bonds to two sulfur atoms, one in each of the adjacent layers, thereby attaining quasi-octahedral coordination. This phase possessed the lowest enthalpy between 100-200 GPa, and it was 28 meV/atom more stable than the $Imma$ SPH_6 structure proposed by Tsuppayakorn-aek and co-workers.[43] It is instructive to compare the geometry of $Amm2$ SPH_6 with CSH_7,[36,37] since the two systems have the same valence electron counts. The family of dynamically stable CSH_7 structures could also be described as being built from 2D S-H square nets separated by CH_4 molecules. But, the smaller radius of carbon relative to phosphorous facilitated the bonding of two adjacent S-H layers via the extra hydrogen atom per formula unit, thereby forming an SH_3 cage within which methane was intercalated.

Finally, a $Pm\bar{3}m$ SPH_2 structure whose unit cell contained a phosphorous atom at the center and faces of the cube, and sulfur atoms at the cube edges and vertices was identified at 200 GPa. The phosphorus atom at the center of the cube was coordinated to eight hydrogen atoms at a distance of 1.593 Å. At lower pressures the most stable EA structures consisted of SP layers terminated and separated by atomic or molecular hydrogen, similar to some of the PH_n phases

previously proposed between 40-100 GPa.[78]

$Im\bar{3}m$ H_3S is a highly symmetric structure where each H-S distance measures 1.492 Å at 200 GPa because of bond symmetrization that occurs under increasing pressure.[95] At relatively low levels of S $\rightarrow$ P substitutions the doped structures retain the same basic lattice, with slight distortions that can be traced back to the atomic size and electronegativity differences between the two p-group elements. With the exception of 12.5% doping, the DOS at E_F of all of the aforementioned cage-like structures was found to be smaller than that of the H_3S parent. Below we will see how chemical substitution affects the propensity for superconductivity of these S-P-H phases.

Structures with 2D Hexagonal Sheets

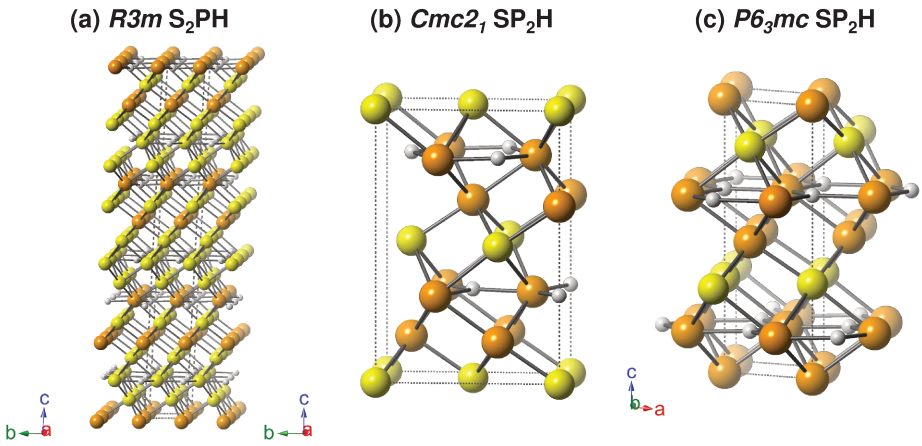

Figure 4: Illustrations of predicted S-P-H phases that contained hexagonal H-S and/or P-H sheets: (a) $R3m$ S_2PH at 200 GPa, (b) $Cmc2_1$ SP_2H at 150 GPa, and (c) $P6_3mc$ SP_2H at 200 GPa. S/P/H atoms are colored yellow/orange/white.

Stoichiometries that differed from those that could be derived by doping H_3S with phosphorous were also explored via evolutionary crystal structure searches. Previous theoretical studies pinpointed a unique $P\bar{6}m2$ $CaSH_3$ phase consisting of alternating CaH_2 and honeycomb H-S sheets

that possessed two vHs bracketing E_F thereby increasing the number of states that can participate in the pairing mechanism, and concomitantly the T_c of this phase.[20] This structure was metastable down to 128 GPa, where its T_c was estimated to be as high as 100 K. Analogous layered structures were identified in this study (Fig. 4), but they could be comprised of either H-P or H-S honeycomb sheets, and some contained both.

For example, $R3m$ S_2PH could be described as a layered structure comprised of H-S and H-P hexagonal nets that were separated from each other by a layer of sulfur atoms (located on top of the centers of the hexagons), or by three S-P-S layers. This structure was just 2.7 meV/atom shy of the 200 GPa convex hull. Whereas the S-H honeycomb nets did not bond with atoms in the adjacent CaH_2 layers in $P\bar{6}m2$ $CaSH_3$,[20] here covalent bonds are formed between the main group elements in the honeycomb sheets and the sulfur atoms in the next layer. Both the H-S and H-P bond lengths in the hexagonal sheets present in $R3m$ S_2PH (1.650 and 1.658 Å) were longer than the one found in $P\bar{6}m2$ $CaSH_3$ (1.605 Å) at 200 GPa. At lower pressures the most stable phases with this stoichiometry did not contain these types of hexagonal layer motifs.

Finally, two different SP_2H structures, both comprised of 2D hexagonal P-H sheets that were separated by a layer of sulfur and a layer of phosphorous atoms lying above or below the hexagonal holes, were found. The main difference between these two phases is that the $Cmc2_1$ structure, stable between 110-170 GPa, possessed two distinct P-H distances (1.643/1.730 Å), whereas all of the P-H distances were equalized in the higher pressure $P6_3/mc$ phase (1.660 Å). These systems lay 22.4 and 54.8 meV/atom above the convex hull at 150 and 200 GPa, respectively.

Structures with 2D Sheets and/or 1D Molecular Chains

In addition to the previously discussed cage-like structures and 2D hexagonal sheets, several metastable phases that contained 2D sheets and/or 1D molecular chains were found in our evolutionary searches. Some examples, illustrated in Fig. 5, include SP_2H_9 and $S_2P_3H_{15}$ (at 150 and 200 GPa), which contained both 1D molecular chains and 2D sheets, SP_3H_{12}, which possessed 2D sheets and $S_2P_3H_{15}$ (at 100 GPa), comprised of 1D molecular chains. Other systems not discussed

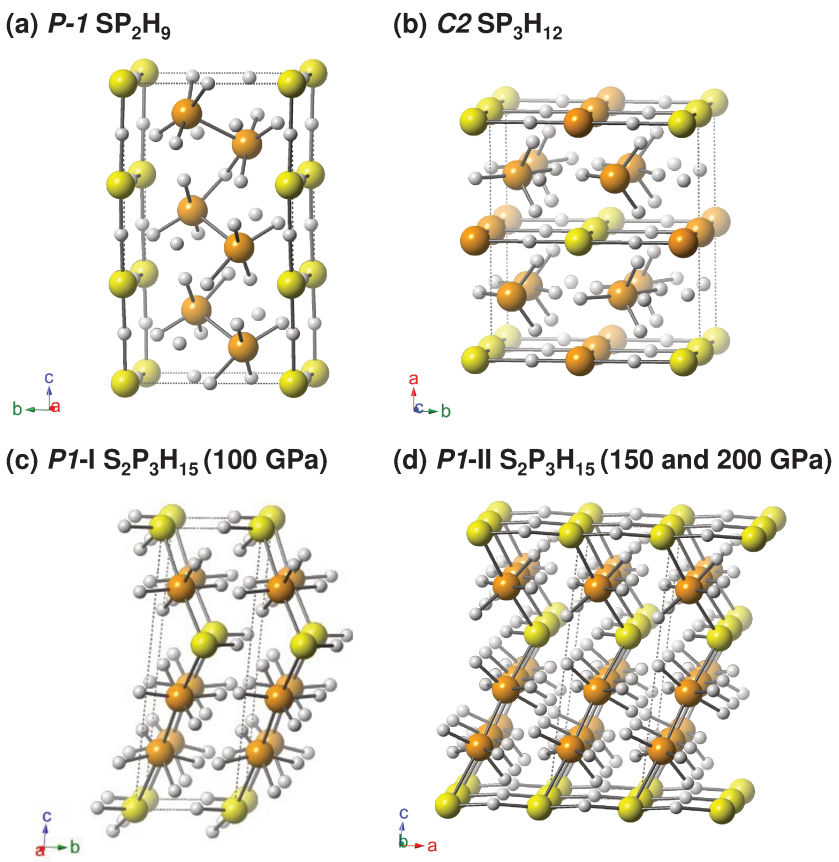

Figure 5: Illustrations of predicted S-P-H phases that contained 2D sheets and/or 1D "nanothreads": (a) $P\bar{1}$ ($S_{0.33}P_{0.67}H_3$) SP_2H_9 at 150 GPa, (b) $C2$ SP_3H_{12} at 100 GPa, (c) $P1$-I $S_2P_3H_{15}$ at 100 GPa, (d) $P1$-II $S_2P_3H_{15}$ at 150 GPa. S/P/H atoms are colored yellow/orange/white.

here (Fig. S42), such as SPH_5 and SP_4H_{15}, only contained 1D molecular chains.

Though phases with the SP_2H_9 stoichiometry were enthalpically unstable with respect to elemental H_2, S and P, their ΔH_F was still within the threshold proposed to gauge the synthesizability of a metastable material at 1 atm.[92] At 100 and 150 GPa the most stable SP_2H_9 geometry adopted a $P\bar{1}$ symmetry structure that contained 2D H-S square nets, where the sulfur atoms comprised the edges and the hydrogen atoms the vertices, extending along the c-axis. These sheets were separated from one another by a layer of H_3P-PH_3 molecular motifs that were linked to each other via an extra hydrogen atom bonded to two phosphorous atoms from adjacent units thereby forming a 1D chain analogous to a nanothread.[96] The bond length between phosphorous and a bridging hydrogen atom was longer than between phosphorous and a terminal hydrogen atom (1.51-1.54 Å vs. 1.36-

1.40 Å at 150 GPa). At 200 GPa the preferred SP_2H_9 structure did not possess any distinguishing features, so it is not discussed here.

Like SP_2H_9, the most stable SP_3H_{12} phases were within the realm of synthesizability even though their enthalpies of formation were positive. At 200 GPa the enthalpy of the most stable structure found at 200 GPa, Cm SP_3H_{12}, was 33 meV/atom lower than that of a previously proposed phase with this stoichiometry, $Immm$ SP_3H_{12} at 200 GPa.[43] However, neither it nor the Cc phase found at lower pressures possessed characteristic structural motifs. Therefore, here we describe the $C2$ phase, which was the ground state structure at 100 GPa. $C2$ SP_2H_9 possessed 2D square nets similar to those found within the previously described $P\bar{1}$ SP_2H_9 phase, except some of the sulfur atoms were replaced by phosphorous. These layers were separated by PH_4 motifs that were within bonding distance to the p-block elements above or below them in the 2D nets.

The most stable $S_2P_3H_{15}$ phase found at 100 GPa can be described as an S-P-H nanothread where each phosphorus atom is octahedrally coordinated to four hydrogen atoms that lie in the same plane and two SH motifs, or to one SH motif and one hydrogen atom. The sulfur atoms in these SH motifs and the hydrogen atoms are bonded to a nearby PH_4 unit. Higher pressures push adjacent nanothreads close enough to form S-H-S bonds along the a axis resulting in a 2D S-H square net that is characteristic of many of these compounds by 150 GPa. Another difference between the preferred $S_2P_3H_{15}$ structures at 150 and 200 GPa is that the hydrogen atom that bridges two phosphorous atoms in the lower pressure phase migrates to the 2D S-H net upon compression.

Phases on the Hull

Our calculations revealed four thermodynamically stable species that lay on the convex hull; these are illustrated in Fig. 6. A $Cmcm$ symmetry SPH phase that was 5.8 meV/atom above the hull at 150 GPa and lay on the hull at 200 GPa possessed. It can be considered as a distorted ZrBeSi-type lattice (e.g. BaAgAs[97]) with the P and H atoms on the Be and Si sites, but the P and H atoms did not form the hexagonal sheets since the P-H distance (1.459/1.728Å) were too long. At lower pressures a $P2_1/m$ symmetry structure, which is not discussed here because it did not present any

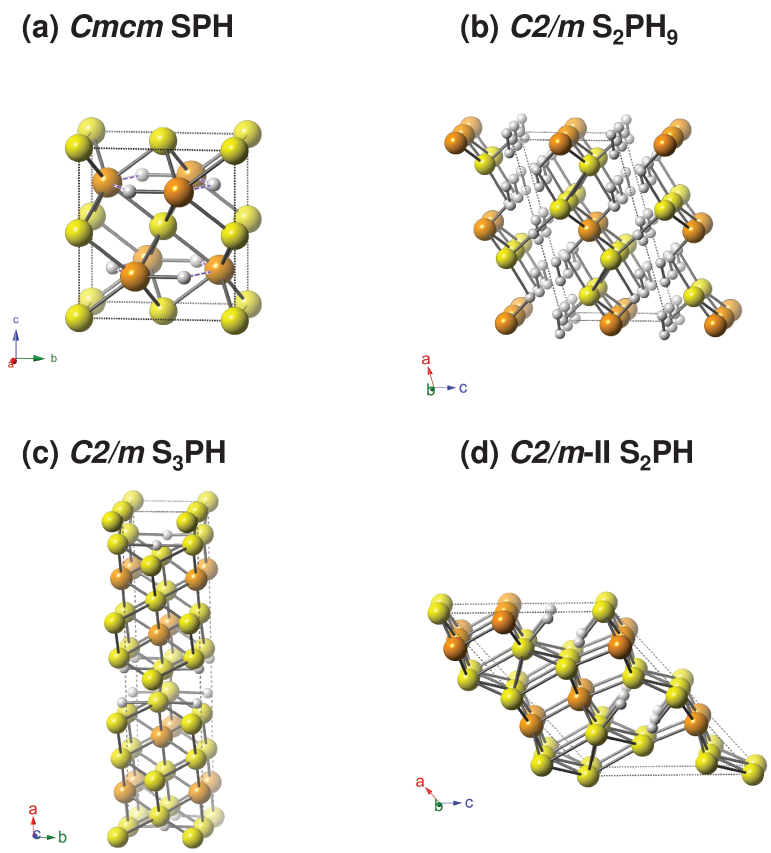

Figure 6: Illustrations of predicted S-P-H phases that lay on the convex hull: (a) $Cmcm$ SPH at 200 GPa (Some P-H are connected by dash lines for better eye-view) , (b) $C2/m$ S_2PH_9 at 100 GPa, (c) $C2/m$ S_3PH at 150 GPa, (d) $C2/m$-II S_2PH at 150 GPa. S/P/H atoms are colored yellow/orange/white.

distinguishing characteristics, was the most stable SPH stoichiometry phase.

S_2PH_9 was the only thermodynamically stable system with a $S_xP_{1-x}H_3$ stoichiometry ($x = 0.67$). It lay on the 100 GPa convex hull, but was 18.6/56.9 meV/atom above the hull at 150/200 GPa. At 100 GPa the preferred structure possessed $C2/m$ symmetry, and it could be derived from adding hydrogen to the most stable S_2P phase found at this pressure.[72] A 1D chain of vertex sharing S-P-S-P rhombii comprised this phase. The phosphorous atoms, which belonged to two rhombii, were octahedrally coordinated to four sulfur atoms and two hydrogen atoms. Each sulfur atom was bonded to a hydrogen atom, which was further bonded to a sulfur atom in an adjacent 1D chain, and H_2 molecules were interspersed between the chains. A $C2/m$ symmetry S_3PH phase lay on the 100 and 150 GPa convex hulls, but it was 25.4 meV/atom above the 200 GPa hull. It could be viewed as a distorted cubic network where phosphorous or sulfur atoms were found on the vertices of the cubes. All of the phosphorus atoms were octahedrally coordinated by bonds to sulfur atoms. Many sulfur atoms were octahedrally coordinated as well, and those that weren't were bonded to hydrogen atoms that were shared between two sulfur atoms. Finally, $C2/m$-II S_2PH was also thermodynamically stable at 150 GPa. It resembled S_3PH, except the octahedrally coordinated phosphorous atoms were bonded to both P and S, some of the sides of the distorted cubes were more like parallelograms, and the hydrogen atoms were only bonded to a single sulfur atom. Both S_2PH and S_3PH could be derived from the most stable high pressure S_2P and S_3P phases that were predicted in previous reports.[72]

Electronic Structure and Superconducting Properties

The PBE electronic band structures and DOS plots of both thermodynamically and dynamically stable S-P-H phases (Figs. S8-26) showed that most were metallic except for $P\bar{1}$ SPH_4 at 100 GPa, Pm SPH_5 at 100-150 GPa, $P1$ S_4PH_{15} ($S_{0.8}P_{0.2}H_3$) at 100 GPa, $C2/m$ S_2PH_9 ($S_{0.67}P_{0.33}H_3$) at 100-200 GPa and $P\bar{1}$ $S_2P_3H_{15}$ ($S_{0.4}P_{0.6}H_3$) at 100 GPa. In general the DOS at the Fermi level in the SPH_n ($n = 1-2$) phases was dominated by the phosphorous and sulfur p states in nearly equivalent proportions. In most of the phases with a larger hydrogen content such as SPH_n ($n = 3-6$) all

three atom types contributed nearly equally to the DOS at E_F, and the most abundant p block element possessed the largest amount of character at E_F in S_xP_yH ($x, y = 2, 3$) phases. For the cage-like doped systems illustrated in Fig. 2 the states at E_F were primarily characterized by sulfur and hydrogen character, whereas those with 2D or 1D motifs (i.e. those in Fig. 5) possessed more hydrogenic character.

A large DOS at E_F is a prerequisite for high T_c, in particular if it results from states related to hydrogen. Another descriptor that can be associated with high temperature conventional superconductors is an increased Debye frequency, which is a consequence of the vibrations of atoms with light masses. Therefore, these quantities were calculated for the metallic S-P-H phases found in our work (Table S3-4) and used to screen for the most likely structures to have a high T_c. If the DOS per valence electron at E_F was calculated to be $\gtrsim$ 0.035 states/eV and the Debye frequency was $\gtrsim$ 750 cm^{-1}, electron phonon coupling (EPC) calculations were performed to probe the superconducting properties of the phase. In addition, EPC calculations were carried out for SPH, SP_2H, S_2PH, S_3PH, SPH_2 and SPH_3 though they did not meet these criteria because their superconducting characteristics could be compared to those previously computed for S-P phases.

Table 2 lists the electron phonon coupling parameter, λ, and logarithmic average of phonon frequencies ($\omega_{\log}$) for the considered phases, as well as their T_cs as estimated via the Allen-Dynes modified McMillan equation. Comparison of our results with the T_cs previously computed[72] for SP, SP_2, and PS_2 (1.5-4.3 K) shows that addition of a single hydrogen atom can raise T_c by an order of magnitude (cf. 17-21 K for SPH and SP_2H) primarily because of an increase in λ. Adding one or two more hydrogen atoms, e.g. to form SPH_2 or SPH_3, does not impact T_c by much, but the T_c of $P2_1/m$ SPH_4 (Fig. S42) was estimated to be significantly larger, 64 K at 200 GPa.

Generally speaking, phases that were constructed by doping $Im\bar{3}m$ H_3S with phosphorous, e.g. those with $S_{1-x}P_xH_3$ stoichiometries, were the best superconductors. The T_c of the most stable 12.5% doped structure at 150 GPa was estimated to be 117 K, which is lower than previous reports for this stoichiometry at the same pressure (168 K[40] and 190 K[42]). However, the structures considered in prior studies were not found using crystal structure prediction techniques and were

at least 7 meV/atom less stable than the phase found here at 150 GPa. The $I4/m$ symmetry 20% doped structure possessed the second highest T_c of any phase we considered (136 K at 200 GPa), decreasing slightly at lower pressures (114 K at 150 GPa within the $I4$ spacegroup). Because the modified McMillan equation is known to underestimate T_c for systems with large EPC values, we also numerically solved the Eliashberg equations for both the 12.5% and 20% dopings. However, comparison of our calculated T_c for $Im\bar{3}m$ H_3S at 200 GPa with experiment ($\sim$175-190 K)[98] shows that when μ^* is chosen to be 0.1, the modified McMillan equation gives values that better agree with those that were measured.

Increasing the doping to 25% decreases T_c to 28/93 K at 150/200 GPa. The drop in T_c with an increase in doping correlates with the decreased DOS at E_F, which is maximal for 12.5% doping. Previously, Durajski and Szcześniak used the supercell approach to propose a 50% doped structure with a T_c of 157 K at 155 GPa,[42] while Tsuppayakornaek *et al.* used crystal structure prediction to find an SPH_6 phase with an estimated T_c of 89 K at 200 GPa.[43] The most stable structure XTALOPT found with this stoichiometry was 70.2 meV/atom lower than the one generated via the supercell approach at 150 GPa, and 28 meV/atom lower than Tsuppayakornaek's structure at 200 GPa. However, the DOS at E_F of our predicted SPH_6 phase was so low that an EPC calculation was not considered. Even though the stoichiometry of Pm SP_2H_9 is compatible with that of a P-doped H_3S structure, the large concentration of phosphorous has a dramatic impact on the geometry of this phase (Fig. S42), which did not show any distinct structural features. Nonetheless, it's estimated T_c, 66 K at 200 GPa, was comparably high.

The superconducting critical temperatures of all of the phases discussed so far are lower than that of the parent $Im\bar{3}m$ H_3S structure. However, as illustrated in Fig. 3, at 200 GPa the DOS at E_F of the $Im\bar{3}m$ S_7PH_{24} phase is slightly higher than that of the undoped structure. Like sulfur, many textbook examples highlight the propensity of phosphorous to assume hypervalent coordination environments so the phase is stable to lower pressures than octahedrally coordinated carbon in O_h-$CS_{15}H_{48}$.[35] Moreover, unlike in the carbon doped phase the hydrogen atoms retain their multi-centered coordination so the metallicity is not decreased.

Table 2: Electron-phonon coupling parameter (λ), logarithmic average of phonon frequencies ($\omega_{\log}$), and estimated superconducting critical temperature (T_c) for a given pressure of various S-P-H phases. The calculations employed the Allen-Dynes modified McMillan equation with a renormalized Coulomb potential, $\mu^* = 0.1$. Values in parentheses were calculated via numerical solution of the Eliashberg equations.

System	Pressure	λ	$\omega_{\log}$ (K)	T_c (K)
$P2_1/m$ SP [a]	100	0.46	522.4	4.3
$C2/m$ SP_2 [a]	150	0.38	506.8	1.5
$C2/m$ PS_2 [a]	100	0.45	453.3	1.7
$P\bar{3}m1$ PS_2 [a]	200	0.37	611.0	1.5
$R3m$ H_3S [b]	130	2.07	1125.1	166
$Im\bar{3}m$ H_3S	200	1.94	1337.0	188.5 (249.2)
$Cmcm$ SPH	200	0.66	724.9	21.9
$Cmc2_1$ SP_2H	150	0.63	615.6	16.3
$C2/m$-II S_2PH	150	0.70	594.3	21.0
$C2/m$ S_3PH	150	0.53	562.7	8.7
Cm SPH_2	150	0.63	738.1	19.5
$P2_1/m$ SPH_3	150	0.57	853.3	17.0
$P2_1/m$ SPH_4	200	0.88	1124.5	63.7
Cm S_7PH_{24} ($S_{0.875}P_{0.125}H_3$)	100	1.06	782.4	59.4
Cm S_7PH_{24} ($S_{0.875}P_{0.125}H_3$)	150	1.42	1081.2	116.8 (147.6)
$Im\bar{3}m$ S_7PH_{24} ($S_{0.875}P_{0.125}H_3$)	200	2.21	1188.1	182.5 (257.5)
$I4$ S_4PH_{15} ($S_{0.8}P_{0.2}H_3$)	150	1.47	1020.5	113.9 (145.9)
$I4/m$ S_4PH_{15} ($S_{0.8}P_{0.2}H_3$)	200	1.42	1259.2	135.9 (171.6)
$Imm2$ S_3PH_{12} ($S_{0.75}P_{0.25}H_3$)	150	0.64	1153.0	27.3
$Immm$ S_3PH_{12} ($S_{0.75}P_{0.25}H_3$)	200	1.08	1187.5	92.6
Pm SP_2H_9 ($S_{0.33}P_{0.67}H_3$)	200	0.99	950.3	65.5

[a] Calculated in Ref.[72] [b] Calculated in Ref.[19]

Previous studies have computed the T_c of $Im\bar{3}m$ S_7PH_{24} and arrived at different conclusions. Durajski and Szcześniak concluded that S→P replacement cannot raise the T_c of H_3S, finding a maximum T_c of 190 K at 155 GPa using the Eliashberg formualism and $\mu^* = 0.15$,[42] but lower level dopings were not considered. At about the same time, Nakanishi and co-workers found that 12.5% doping increases the T_c of H_3S at 200 GPa from 189 to 194 K using the Allen-Dynes modified McMillan equation with strong coupling and shape factors, and from 225 to 249 K using the isotropic Eliashberg equation with $\mu^* = 0.13$.[40] Even higher T_cs (212 and 268 K via the Allen-Dynes and Eliashberg methods, respectively) were computed for 6.5% doping levels. Most recently, Guan and colleagues reported that 12.5% phosphorous content barely changes the T_c of

H_3S at 200 GPa.[41] A decreased doping of 6.5%, on the other hand, increased the T_c of at 200 GPa from 214 to 231 K using the Allen-Dynes modified McMillan equation with strong coupling and shape factors, and from 238 to 262 K via Migdal-Eliashberg theory with $\mu^* = 0.1$.[41]

Our results echo those of Guan and co-workers: at 200 GPa the estimated T_c of $Im\bar{3}m$ S_7PH_{24} differs by 6-8 K from the value predicted for $Im\bar{3}m$ H_3S, which is within our calculation error. Therefore, we conclude that the 12.5% doping of H_3S by phosphorous does not change T_c by much. While Guan and Nakanishi both found that 6.25% doping increased the T_c relative to that of $Im\bar{3}m$ H_3S slightly, this system was not considered here because its DOS at E_F was calculated to be lower than that of $Im\bar{3}m$ S_7PH_{24} at 200 GPa (Fig. S7). Interestingly, the highest T_c structure we found, $Im\bar{3}m$ S_7PH_{24}, possessed cubic symmetry, similar to other high-T_c phases including $Im\bar{3}m$ H_3S,[19] $Fm\bar{3}m$ LaH10[21,22] and $Fd\bar{3}m$ Li_2MgH_{16}.[24] Since high symmetry structures possess degenerate bands, they may have a large DOS at E_F, thereby enhancing λ and the resulting T_c.

Conclusions

The exciting discovery of novel hydride-based superconductors with record breaking superconducting critical temperatures, T_cs, has fueled the search for evermore complex systems. One way to design new superconducting materials is by doping known structures in the hopes of finding a material with a higher T_c, or a lower stabilization pressure. Previous studies have consider the effect of phosphorous doping on the T_c of $Im\bar{3}m$ H_3S, however they were performed either using the virtual crystal approximation or they only considered phases derived from S→P replacement within the $Im\bar{3}m$ H_3S parent.

To overcome these limitations we have employed crystal structure prediction techniques to explore a wide $S_xP_yH_z$ composition range. The convex hull was mapped out under pressure and found to consist of $Cmcm$ SPH (200 GPa), $C2/m$ S_2PH_9 (100 GPa), $C2/m$ S_3PH (100, 150 GPa) and $C2/m$-II S_2PH (150 GPa). Of these phases, the ones whose T_cs were calculated ranged from 9-22 K. In addition, a wide variety of potentially synthesizable compounds were predicted contain-

ing unique structural motifs such as one-dimensional nanothreads, two-dimensional square nets or honeycomb sheets, as well as cages. From the cages, those with the highest T_cs corresponded to low dopings of $Im\bar{3}m$ H_3S with phosphorous. The propensity for phosphorous to participate in hypervalent bonds coupled to its similar-to-sulfur-size were key to retaining a high density of states at the Fermi level in $Im\bar{3}m$ S_7PH_{24} ($S_{0.875}P_{0.125}H_3$), whose T_c was predicted to be 183 K at 200 GPa. We hope this study inspires the eventual synthesis of these compounds, and the exploration of their physical and chemical behavior.

Supporting Information: The Supporting Information is available free of charge on the ACS Publication website. It includes the space group at various pressures, distance above the convex-hull, the structural parameters, relative enthalpies, equation of states, electronic band structures and densities of states, electron localization functions, phonon density of states, computational parameters in EPC calculations, superconducting properties of selected phases, and illustrations of crystal structure of other S-P-H ternary phases.

Acknowledgements: We acknowledge the U.S. National Science Foundation (DMR-1827815) for financial support. Calculations were performed at the Center for Computational Research at SUNY Buffalo.[99]

References

(1) Ashcroft, N. W. Metallic Hydrogen: A High–Temperature Superconductor? *Phys. Rev. Lett.* **1968**, *21*, 1748–1749.

(2) Ashcroft, N. W. Hydrogen Dominant Metallic Alloys: High Temperature Superconductors? *Phys. Rev. Lett.* **2004**, *92*, 187002.

(3) Drozdov, A. P.; Eremets, M. I.; Troyan, I. A.; Ksenofontov, V.; Shylin, S. I. Conventional

Superconductivity at 203 Kelvin at High Pressures in the Sulfur Hydride System. *Nature* **2015**, *525*, 73–76.

(4) Somayazulu, M.; Ahart, M.; Mishra, A. K.; Geballe, Z. M.; Baldini, M.; Meng, Y.; Struzhkin, V. V.; Hemley, R. J. Evidence for Superconductivity above 260 K in Lanthanum Superhydride at Megabar Pressures. *Phys. Rev. Lett.* **2019**, *122*, 027001.

(5) Drozdov, A. P.; Kong, P. P.; Minkov, V. S.; Besedin, S. P.; Kuzovnikov, M. A.; Mozaffari, S.; Balicas, L.; Balakirev, F. F.; Graf, D. E.; Prakapenka, V. B. et al. Superconductivity at 250 K in Lanthanum Hydride Under High Pressures. *Nature* **2019**, *569*, 528–531.

(6) Troyan, I. A.; Semenok, D. V.; Kvashnin, A. G.; Sadakov, A. V.; Sobolevskiy, O. A.; Pudalov, V. M.; Ivanova, A. G.; Prakapenka, V. B.; Greenberg, E.; Gavriliuk, A. G. et al. Anomalous High–Temperature Superconductivity in YH_6. *Adv. Mater.* **2021**, *33*, 2006832.

(7) Kong, P.; Minkov, V. S.; Kuzovnikov, M. A.; Drozdov, A. P.; Besedin, S. P.; Mozaffari, S.; Balicas, L.; Balakirev, F. F.; Prakapenka, V. B.; Chariton, S. et al. Superconductivity up to 243 K in the Yttrium–Hydrogen System Under High Pressure. *Nat. Commun.* **2021**, *12*, 5075.

(8) Snider, E.; Dasenbrock-Gammon, N.; McBride, R.; Wang, X.; Meyers, N.; Lawler, K. V.; Zurek, E.; Salamat, A.; Dias, R. P. Synthesis of Yttrium Superhydride Superconductor with a Transition Temperature up to 262 K by Catalytic Hydrogenation at High Pressures. *Phys. Rev. Lett.* **2021**, *126*, 117003.

(9) Snider, E.; Dasenbrock-Gammon, N.; McBride, R.; Debessai, M.; Vindana, H.; Vencatasamy, K.; Lawler, K. V.; Salamat, A.; Dias, R. P. Room–Temperature Superconductivity in a Carbonaceous Sulfur Hydride. *Nature* **2020**, *586*, 373–377.

(10) Zurek, E.; Grochala, W. Predicting Crystal Structures and Properties of Matter Under Extreme Conditions via Quantum Mechanics: The Pressure is On. *Phys. Chem. Chem. Phys.* **2015**, *17*, 2917–2934.

(11) Miao, M.; Sun, Y.; Zurek, E.; Lin, H. Chemistry Under High Pressure. *Nat. Rev. Chem.* **2020**, *508–527*, 4.

(12) Flores-Livas, J. A.; Boeri, L.; Sanna, A.; Profeta, G.; Arita, R.; Eremets, M. A Perspective on Conventional High–Temperature Superconductors at High Pressure: Methods and Materials. *Phys. Rep.* **2020**, *856*, 1–78.

(13) Bi, T.; Zarifi, N.; Terpstra, T.; Zurek, E. $Reference\ Module\ in\ Chemistry,\ Molecular\ Sciences\ and\ Chemical\ Engineering$; Elsevier Ltd., 2019; pp 1–36.

(14) Wang, H.; Li, X.; Gao, G.; Li, Y.; Ma, Y. Hydrogen-Rich Superconductors at High Pressures. *Wiley Interdiscip. Rev.: Comput. Mol. Sci.* **2018**, *8*, e1330.

(15) Zurek, E.; Bi, T. High–Temperature Superconductivity in Alkaline and Rare Earth Polyhydrides at High Pressure: A Theoretical Perspective. *J. Chem. Phys.* **2019**, *150*, 050901.

(16) Boeri, L.; Hennig, R. G.; Hirschfeld, P. J.; Profeta, G.; Sanna, A.; Zurek, E.; Pickett, W. E.; Amsler, M.; Dias, R.; Eremets, M. et al. The 2021 Room–Temperature Superconductivity Roadmap. *J. Phys.: Condens. Matter* **2021**, "in press" DOI: 10.1088/1361-648X/ac2864.

(17) Hilleke, K. P.; Zurek, E. Tuning Chemical Precompression: Theoretical Design and Crystal Chemistry of Novel Hydrides in the Quest for Warm and Light Superconductivity at Ambient Pressures. *J. Appl. Phys.* **2022**, *131*, 070901.

(18) Wang, H.; Tse, J. S.; Tanaka, K.; Iitaka, T.; Ma, Y. Superconductive Sodalite–Like Clathrate Calcium Hydride at High Pressures. *Proc. Natl. Acad. Sci. U.S.A.* **2012**, *109*, 6463–6466.

(19) Duan, D.; Liu, Y.; Tian, F.; Li, D.; Huang, X.; Zhao, Z.; Yu, H.; Liu, B.; Tian, W.; Cui, T. Pressure–Induced Metallization of Dense $(H_2S)_2H_2$ with High–T_c Superconductivity. *Sci. Rep.* **2014**, *4*, 6968.

(20) Yan, Y.; Bi, T.; Geng, N.; Wang, X.; Zurek, E. A Metastable $CaSH_3$ Phase Composed of HS

Honeycomb Sheets that is Superconducting Under Pressure. *J. Phys. Chem. Lett.* **2020**, *11*, 9629–9636.

(21) Peng, F.; Sun, Y.; Pickard, C. J.; Needs, R. J.; Wu, Q.; Ma, Y. Hydrogen Clathrate Structures in Rare Earth Hydrides at High Pressures: Possible Route to Room–Temperature Superconductivity. *Phys. Rev. Lett.* **2017**, *119*, 107001.

(22) Liu, H.; Naumov, I. I.; Hoffmann, R.; Ashcroft, N. W.; Hemley, R. J. Potential High–T_c Superconducting Lanthanum and Yttrium Hydrides at High Pressure. *Proc. Natl. Acad. Sci. U.S.A.* **2017**, *114*, 6990–6995.

(23) Semenok, D. V.; Troyan, I. A.; Ivanova, A. G.; Kvashnin, A. G.; Kruglov, I. A.; Hanfland, M.; Sadakov, A. V.; Sobolevskiy, O. A.; Pervakov, K. S.; Lyubutin, I. S. et al. Superconductivity at 253 K in Lanthanum–Yttrium Ternary Hydrides. *Mater. Today* **2021**, *48*, 18–28.

(24) Sun, Y.; Lv, J.; Xie, Y.; Liu, H.; Ma, Y. Route to a Superconducting Phase above Room Temperature in Electron–Doped Hydride Compounds Under High Pressure. *Phys. Rev. Lett.* **2019**, *123*, 097001.

(25) Lonie, D. C.; Hooper, J.; Altintas, B.; Zurek, E. Metallization of Magnesium Polyhydrides Under Pressure. *Phys. Rev. B* **2013**, *87*, 054107.

(26) Di Cataldo, S.; Heil, C.; von der Linden, W.; Boeri, L. $LaBH_8$: Towards High–T_c Low–Pressure Superconductivity in Ternary Superhydrides. *Phys. Rev. B* **2021**, *104*, L020511.

(27) Liang, X.; Bergara, A.; Wei, X.; Song, X.; Wang, L.; Sun, R.; Liu, H.; Hemley, R. J.; Wang, L.; Gao, G. et al. Prediction of High–T_c Superconductivity in Ternary Lanthanum Borohydrides. *Phys. Rev. B* **2021**, *104*, 134501.

(28) Zhang, Z.; Cui, T.; Hutcheon, M. J.; Shipley, A. M.; Song, H.; Du, M.; Kresin, V. Z.; Duan, D.; Pickard, C. J.; Yao, Y. Design Principles for High Temperature Superconductors

with a Hydrogen–Based Alloy Backbone at Moderate Pressure. *Phys. Rev. Lett.* **2022**, *128*, 047001.

(29) Heil, C.; Boeri, L. Influence of Bonding on Superconductivity in High–Pressure Hydrides. *Phys. Rev. B* **2015**, *92*, 060508(R).

(30) Ge, Y.; Zhang, F.; Yao, Y. First–Principles Demonstration of Superconductivity at 280 K in Hydrogen Sulfide with Low Phosphorus Substitution. *Phys. Rev. B* **2016**, *93*, 224513.

(31) Ge, Y.; Zhang, F.; Dias, R. P.; Hemley, R. J.; Yao, Y. Hole–Doped Room–Temperature Superconductivity in $H_3S_{1-x}Z_x$ (Z=C, Si). *Mater. Today Phys.* **2020**, *15*, 100330.

(32) Hu, S. X.; Paul, R.; Karasiev, V. V.; Dias, R. P. Carbon–Doped Sulfur Hydrides as Room–Temperature Superconductors at 270 GPa. *arXiv preprint* **2020**, arXiv:2012.10259.

(33) Fan, F.; Papaconstantopoulos, D. A.; Mehl, M. J.; Klein, B. M. High–Temperature Superconductivity at High pressures for $H_3Si_xP_{1-x}$, $H_3P_xS_{1-x}$, and $H_3Cl_xS_{1-x}$. *J. Phys. Chem. Solids* **2016**, *99*, 105–110.

(34) Wang, T.; Hirayama, M.; Nomoto, T.; Koretsune, T.; Arita, R.; Flores-Livas, J. A. Absence of Conventional Room–Temperature Superconductivity at High Pressure in Carbon–Doped H_3S. *Phys. Rev. B* **2021**, *104*, 064510.

(35) Wang, X.; Bi, T.; Hilleke, K. P.; Lamichhane, A.; Hemley, R. J.; Zurek, E. A Little Bit of Carbon Can Do a Lot for Superconductivity in H_3S. *arXiv preprint* **2021**, arXiv:2109.09898v2.

(36) Sun, Y.; Tian, Y.; Jiang, B.; Li, X.; Li, H.; Iitaka, T.; Zhong, X.; Xie, Y. Computational Discovery of a Dynamically Stable Cubic SH_3–Like High–Temperature Superconductor at 100 GPa via CH_4 Intercalation. *Phys. Rev. B* **2020**, *101*, 174102.

(37) Cui, W.; Bi, T.; Shi, J.; Li, Y.; Liu, H.; Zurek, E.; Hemley, R. J. Route to High–T_c Superconductivity via CH_4–Intercalated H_3S Hydride Perovskites. *Phys. Rev. B* **2020**, *101*, 134504.

(38) Amsler, M. Thermodynamics and Superconductivity of $S_xSe_{1-x}H_3$. *Phys. Rev. B* **2019**, *99*, 060102(R).

(39) Liu, B.; Cui, W.; Shi, J.; Zhu, L.; Chen, J.; Lin, S.; Su, R.; Ma, J.; Yang, K.; Xu, M. et al. Effect of Covalent Bonding on the Superconducting Critical Temperature of the H–S–Se System. *Phys. Rev. B* **2018**, *98*, 174101.

(40) Nakanishi, A.; Ishikawa, T.; Shimizu, K. First–Principles Study on Superconductivity of P– and Cl–Doped H_3S. *J. Phys. Soc. Jpn.* **2018**, *87*, 124711.

(41) Guan, H.; Sun, Y.; Liu, H. Superconductivity of H_3S Doped with Light Elements. *Phys. Rev. Res.* **2021**, *3*, 043102.

(42) Durajski, A. P.; Szczęśniak, R. Gradual Reduction of the Superconducting Transition Temperature of H_3S by Partial Replacing Sulfur with Phosphorus. *Physica C* **2018**, *554*, 38–43.

(43) Tsuppayakorn-aek, P.; Phansuke, P.; Kaewtubtim, P.; Ahuja, R.; Bovornratanaraks, T. Enthalpy Stabilization of Superconductivity in an Alloying S–P–H System: First–Principles Cluster Expansion Study Under High Pressure. *Comput. Mater. Sci.* **2021**, *190*, 110282.

(44) Lonie, D. C.; Zurek, E. XtalOpt: An Open–Source Evolutionary Algorithm for Crystal Structure Prediction. *Comput. Phys. Commun.* **2011**, *182*, 372–387.

(45) XTALOPT Evolutionary Crystal Structure Prediction. http://xtalopt.github.io/ (accessed Feb 22nd, 2022).

(46) Falls, Z.; Avery, P.; Wang, X.; Hilleke, K. P.; Zurek, E. The XtalOpt Evolutionary Algorithm for Crystal Structure Prediction. *J. Phys. Chem. C* **2021**, *125*, 1601–1620.

(47) Avery, P.; Toher, C.; Curtarolo, S.; Zurek, E. XtalOpt Version r12: An Open–Source Evolutionary Algorithm for Crystal Structure Prediction. *Comput. Phys. Commun.* **2019**, *237*, 274–275.

(48) Avery, P.; Zurek, E. RandSpg: An Open–Source Program for Generating Atomistic Crystal Structures with Specific Spacegroups. *Comput. Phys. Commun.* **2017**, *213*, 208–216.

(49) Lonie, D. C.; Zurek, E. Identifying Duplicate Crystal Structures: XtalComp, An Open–Source solution. *Comput. Phys. Commun.* **2012**, *183*, 690–697.

(50) Kresse, G.; Hafner, J. *Ab initio* Molecular Dynamics for Liquid Metals. *Phys. Rev. B.* **1993**, *47*, 558–561.

(51) Kresse, G.; Joubert, D. From Ultrasoft Pseudopotentials to the Projector Augmented–Wave Method. *Phys. Rev. B.* **1999**, *59*, 1758–1775.

(52) Perdew, J. P.; Burke, K.; Ernzerhof, M. Generalized Gradient Approximation Made Simple. *Phys. Rev. Lett.* **1996**, *77*, 3865–3868.

(53) Maintz, S.; Deringer, V. L.; Tchougréeff, A. L.; Dronskowski, R. LOBSTER: A Tool to Extract Chemical Bonding from Plane–Wave Based DFT. *J. Comput. Chem.* **2016**, *37*, 1030–1035.

(54) Blöchl, P. E. Projector Augmented–Wave Method. *Phys. Rev. B* **1994**, *50*, 17953–17979.

(55) Parlinski, K.; Li, Z. Q.; Kawazoe, Y. First–Principles Determination of the Soft Mode in Cubic ZrO_2. *Phys. Rev. Lett.* **1997**, 4063–4066.

(56) Chaput, L.; Togo, A.; Tanaka, I.; Hug, G. Phonon–Phonon Interactions in Transition Metals. *Phys. Rev. B* **2011**, *84*, 094302.

(57) Togo, A.; Tanaka, I. First Principles Phonon Calculations in Materials Science. *Scr. Mater.* **2015**, *108*, 1–5.

(58) Giannozzi, P.; Baroni, S.; Bonini, N.; Calandra, M.; Car, R.; Cavazzoni, C.; Ceresoli, D.; Chiarotti, G. L.; Cococcioni, M.; Dabo, I. et al. QUANTUM ESPRESSO: A Modular and Open–Source Software Project for Quantum Simulations of Materials. *J. Phys.: Condens. Matter* **2009**, *21*, 395502.

(59) Dal Corso, A. Pseudopotentials Periodic Table: From H to Pu. *Comput. Mater. Sci.* **2014**, *95*, 337–350.

(60) Troullier, N.; Martins, J. L. Efficient Pseudopotentials for Plane–Wave Calculations. *Phys. Rev. B* **1991**, *43*, 1993–2006.

(61) Methfessel, M.; Paxton, A. T. High–Precision Sampling for Brillouin–Zone Integration in Metals. *Phys. Rev. B* **1989**, *40*, 3616–3621.

(62) Allen, P. B.; Dynes, R. C. Transition Temperature of Strong–Coupled Superconductors Reanalyzed. *Phys. Rev. B* **1975**, *12*, 905–922.

(63) Eliashberg, G. M. Interactions Between Electrons and Lattice Vibrations in a Superconductor. *Sov. Phys. JETP* **1960**, *11*, 696–702.

(64) Jamieson, J. C. Crystal Structures Adopted by Black Phosphorus at High Pressures. *Science* **1963**, *139*, 1291–1292.

(65) Kikegawa, T.; Iwasaki, H. An X–ray Diffraction Study of Lattice Compression and Phase Transition of Crystalline Phosphorus. *Acta. Cryst.* **1983**, *B39*, 158–164.

(66) Akahama, Y.; Kobayashi, M.; Kawamura, H. Simple-Cubic–Simple-Hexagonal Transition in Phosphorus Under Pressure. *Phys. Rev. B* **1999**, *59*, 8520–8525.

(67) Pickard, C. J.; Needs, R. J. Structure of Phase III of Solid Hydrogen. *Nat. Phys.* **2007**, *3*, 473–476.

(68) Luo, H.; Greene, R. G.; Ruoff, A. L. β-Po Phase of Sulfur at 162 GPa: X–ray Diffraction Study to 212 GPa. *Phys. Rev. Lett.* **1993**, *71*, 2943–2946.

(69) Zakharov, O.; Cohen, M. L. Theory of Structural, Electronic, Vibrational, and Superconducting Properties of High–Pressure Phases of Sulfur. *Phys. Rev. B* **1995**, *52*, 12572–12578.

(70) Gavryushkin, P. N.; Litasov, K. D.; Dobrosmislov, S. S.; Popov, Z. I. High–Pressure Phases of Sulfur: Topological Analysis and Crystal Structure Prediction. *Phys. Status Solidi B* **2017**, *254*, 1600857.

(71) Kokail, C.; Heil, C.; Boeri, L. Search for High–T_c Conventional Superconductivity at Megabar Pressures in the Lithium-Sulfur System. *Phys. Rev. B* **2016**, *94*, 060502(R).

(72) Liu, Y.; Wang, C.; Chen, X.; Lv, P.; Sun, H.; Duan, D. Pressure–Induced Structures and Properties in P–S compounds. *Solid State Commun.* **2019**, *293*, 6–10.

(73) Li, Y.; Wang, L.; Liu, H.; Zhang, Y.; Hao, J.; Pickard, C. J.; Nelson, J. R.; Needs, R. J.; Li, W.; Huang, Y. et al. Dissociation Products and Structures of Solid H_2S at Strong Compression. *Phys. Rev. B* **2016**, *93*, 020103(R).

(74) Kruglov, I.; Akashi, R.; Yoshikawa, S.; Oganov, A. R.; Esfahani, M. M. D. Refined Phase Diagram of the H–S System with High–T_c Superconductivity. *Phys. Rev. B* **2017**, *96*, 220101(R).

(75) Errea, I.; Calandra, M.; Pickard, C. J.; Nelson, J.; Needs, R. J.; Li, Y.; Liu, H.; Zhang, Y.; Ma, Y.; Mauri, F. High–Pressure Hydrogen Sulfide from First Principles: A Strongly Anharmonic Phonon-mediated Superconductor. *Phys. Rev. Lett.* **2015**, *114*, 157004.

(76) Goncharov, A. F.; Lobanov, S. S.; Kruglov, I.; Zhao, X.-M.; Chen, X.-J.; Oganov, A. R.; Konôpková, Z.; Prakapenka, V. B. Hydrogen Sulfide at High Pressure: Change in Stoichiometry. *Phys. Rev. B* **2016**, *93*, 174105.

(77) Mishra, A. K.; Muramatsu, T.; Liu, H.; Geballe, Z. M.; Somayazulu, M.; Ahart, M.; Baldini, M.; Meng, Y.; Zurek, E.; Hemley, R. J. New Calcium Hydrides with Mixed Atomic and Molecular Hydrogen. *J. Phys. Chem. C* **2018**, *122*, 19370–19378.

(78) Bi, T.; Miller, D. P.; Shamp, A.; Zurek, E. Superconducting Phases of Phosphorus Hydride Under Pressure: Stabilization via Mobile Molecular Hydrogen. *Angew. Chem., Int. Ed.* **2017**, *56*, 10192–10195.

(79) Shamp, A.; Terpstra, T.; Bi, T.; Falls, Z.; Avery, P.; Zurek, E. Decomposition Products of Phosphine Under Pressure: PH_2 Stable and Superconducting? *J. Am. Chem. Soc.* **2016**, *138*, 1884–1892.

(80) Flores-Livas, J. A.; Amsler, M.; Heil, C.; Sanna, A.; Boeri, L.; Profeta, G.; Wolverton, C.; Goedecker, S.; Gross, E. K. U. Superconductivity in Metastable Phases of Phosphorus-Hydride Compounds Under High Pressure. *Phys. Rev. B* **2016**, *93*, 020508(R).

(81) Drozdov, A. P.; Eremets, M. I.; Troyan, I. A. Superconductivity above 100 K in PH_3 at High Pressures. *arXiv preprint* **2015**, arXiv:1508.06224.

(82) Ceppatelli, M.; Demetrio, S.; Serrano-Ruiz, M.; Dziubek, K.; Garbarino, G.; Jacobs, J.; Mezouar, M.; Bini, R.; Peruzzini, M. High Pressure Synthesis of Phosphine from the Elements and the Discovery of the Missing $(PH_3)_2H_2$ Tile. *Nat. Commun.* **2020**, *11*, 6125.

(83) Yao, Y.; Tse, J. S. Superconducting Hydrogen Sulfide. *Chem. - Eur. J.* **2018**, *24*, 1769–1778.

(84) Verma, A. K.; Modak, P. A Unique Metallic Phase of H_3S at High–Pressure: Sulfur in Three Different Local Environments. *Phys. Chem. Chem. Phys.* **2018**, *20*, 26344–26350.

(85) Li, Y.; Hao, J.; Liu, H.; Li, Y.; Ma, Y. The Metallization and Superconductivity of Dense Hydrogen Sulfide. *J. Chem. Phys.* **2014**, *140*, 174712.

(86) Akashi, R.; Kawamura, M.; Tsuneyuki, S.; Nomura, Y.; Arita, R. First–Principles Study of the Pressure and Crystal–Structure Dependences of the Superconducting Transition Temperature in Compressed Sulfur Hydrides. *Phys. Rev. B* **2015**, *91*, 224513.

(87) Ishikawa, T.; Nakanishi, A.; Shimizu, K.; Katayama-Yoshida, H.; Oda, T.; Suzuki, N. Superconducting H_5S_2 Phase in Sulfur–Hydrogen System Under High–Pressure. *Sci. Rep.* **2016**, *6*, 23160.

(88) Akashi, R.; Sano, W.; Arita, R.; Tsuneyuki, S. Possible "Magnéli" Phases and Self-Alloying in the Superconducting Sulfur Hydride. *Phys. Rev. Lett.* **2016**, *117*, 075503.

(89) Gordon, E. E.; Xu, K.; Xiang, H.; Bussmann-Holder, A.; Kremer, R. K.; Simon, A.; Köhler, J.; Whangbo, M.-H. Structure and Composition of the 200 K–Superconducting Phase of H_2S at Ultrahigh Pressure: The Perovskite $(SH^-)(H_3S^+)$. *Angew. Chem., Int. Ed.* **2016**, *55*, 3682–3684.

(90) Majumdar, A.; Tse, J. S.; Yao, Y. Modulated Structure Calculated for Superconducting Hydrogen Sulfide. *Angew. Chem., Int. Ed.* **2017**, *56*, 11390–11393.

(91) Majumdar, A.; Tse, J. S.; Yao, Y. Mechanism for the Structural Transformation to the Modulated Superconducting Phase of Compressed Hydrogen Sulfide. *Sci. Rep.* **2019**, *9*, 5023.

(92) Sun, W.; Dacek, S. T.; Ong, S. P.; Hautier, G.; Jain, A.; Richards, W. D.; Gamst, A. C.; Persson, K. A.; Ceder, G. The Thermodynamic Scale of Inorganic Crystalline Metastability. *Sci. Adv.* **2016**, *2*, e1600225.

(93) Novel Materials Discovery. https://nomad-lab.eu/ DOI:https://dx.doi.org/10.17172/NOMAD/2022.02.22-1 (accessed Feb 22nd, 2022).

(94) Toher, C.; Oses, C.; Hicks, D.; Curtarolo, S. Unavoidable Disorder and Entropy in Multicomponent Systems. *npj Comput. Mater.* **2019**, *5*, 69.

(95) Zurek, E. The Pressing Role of Theory in Studies of Compressed Matter. In $Handbook\ of\ Solid\ State\ Chemistry$; Wiley-VCH Verlag GmbH & Co.: Weinheim, Germany, 2017; Vol. 5, pp 571-605.

(96) Li, X.; Baldini, M.; Wang, T.; Chen, B.; Xu, E. S.; Vermilyea, B.; Crespi, V. H.; Hoffmann, R.; Molaison, J. J.; Tulk, C. A. et al. Mechanochemical Synthesis of Carbon Nanothread Single Crystals. *J. Am. Chem. Soc.* **2017**, *139*, 16343–16349.

(97) Mardanya, S.; Singh, B.; Huang, S.-M.; Chang, T.-R.; Su, C.; Lin, H.; Agarwal, A.; Bansil, A. Prediction of Threefold Fermions in a Nearly Ideal Dirac Semimetal BaAgAs. *Phys. Rev. Mater.* **2019**, *3*, 071201(R).

(98) Minkov, V. S.; Prakapenka, V. B.; Greenberg, E.; Eremets, M. I. A Boosted Critical Temperature of 166 K in Superconducting D_3S Synthesized from Elemental Sulfur and Hydrogen. *Angew. Chem., Int. Ed.* **2020**, *59*, 18970–18974.

(99) Center for Computational Research, University at Buffalo. http://hdl.handle.net/10477/79221 (accessed Feb 22nd, 2022).

TOC Graphic

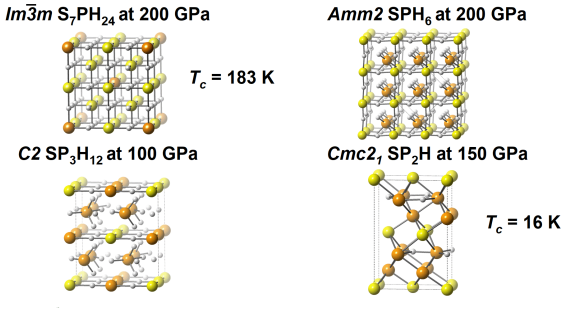
$Im\bar{3}m$ S_7PH_{24} at 200 GPa
T_c = 183 K
$Amm2$ SPH_6 at 200 GPa
$C2$ SP_3H_{12} at 100 GPa
$Cmc2_1$ SP_2H at 150 GPa
T_c = 16 K